ORNL/NRC/LTR-99/26

Contract Program or Project Title:	Heavy-Section Steel Technology (HSST) Program Engineering Technology Division
Subject of this Document:	Comparison of K_I Factors for Embedded Flaws: FAVOR Implementation of ASME Section XI – Appendix A Methodology versus Three-Dimensional Finite-Element Solutions
Type of Document:	Letter Report
Authors:	B. R. Bass P. T. Williams T. L. Dickson G. E. Giles, Jr. W. J. McAfee
Date Published:	April 2000
Responsible NRC Individual and NRC Office or Division	S. N. M. Malik / M. T. Kirk Division of Engineering Technology Office of Nuclear Regulatory Research

Prepared for the
U. S. Nuclear Regulatory Commission
Washington, D.C. 20555-0001
Under Interagency Agreement DOE 1886-N011-9B
NRC JCN No. B0119

OAK RIDGE NATIONAL LABORATORY
Oak Ridge, Tennessee 37831-8063
managed and operated by
UT-Battelle, LLC
for the
U. S. DEPARTMENT OF ENERGY
under Contract No. DE-AC05-00OR22725

ORNL/NRC/LTR-99/26

Comparison of K_I Factors for Embedded Flaws: FAVOR Implementation of ASME Section XI – Appendix A Methodology versus Three-Dimensional Finite-Element Solutions

B. R. Bass, P. T. Williams, T. L. Dickson,
G. E. Giles, Jr., and W. J. McAfee
Oak Ridge National Laboratory
Oak Ridge, Tennessee

Manuscript Completed – October 1999
Date Published – April 2000

Prepared for the
U.S. Nuclear Regulatory Commission
Office of Nuclear Regulatory Research
Under Interagency Agreement DOE 1886-N011-9B

NRC JCN No. B0119

OAK RIDGE NATIONAL LABORATORY
Oak Ridge, Tennessee 37831-8063
managed and operated by
UT-Battelle, LLC
for the
U.S. DEPARTMENT OF ENERGY
under Contract No. DE-AC05-00OR22725

Comparison of K_I Factors for Embedded Flaws: FAVOR Implementation of ASME Section XI –Appendix A Methodology versus Three-Dimensional Finite-Element Solutions

B. R. Bass, P. T. Williams, T. L. Dickson,
G. E. Giles, Jr., and W. J. McAfee

Oak Ridge National Laboratory
P. O. Box 2009
Oak Ridge, TN, 37831-8063

Abstract: This report describes a benchmarking study that compared embedded-flaw K_I stress-intensity factors calculated by the FAVOR computer program with two other independently-developed computer models. A set of K_I versus time solutions were generated for a matrix of subsurface flaws embedded in a reactor pressure vessel (RPV) wall subjected to pressurized-thermal-shock (PTS) conditions. FAVOR employs the subsurface elliptical flaw model presented in the ASME Boiler and Pressure Vessel Code, (Section XI, Appendix A) to calculate applied K_I factors. A second computer program was developed for this study to benchmark the EPRI NP-1181 parametric representation of the Section XI, Appendix A, subsurface-flaw model implemented in FAVOR. Additionally, the ABAQUS computer program was employed to carry out three-dimensional (3-D) finite-element analyses, based on linear-elastic fracture mechanics (LEFM) techniques, of the embedded-flaw test matrix. The ASME Code calculations for embedded flaws were generated by a developmental version of the FAVOR code that incorporates the EPRI analytical interpretation of the ASME Section XI-Appendix A methodology. Comparisons of the results were used to evaluate the ASME model, as implemented in FAVOR, for fracture assessment of embedded flaws. From previous analyses, the primary region of interest regarding embedded flaws is 1/8th of the RPV wall nearest the clad/base metal interface. The current results show that FAVOR calculates applied K_I solutions for embedded flaws that agree closely with the two benchmark solutions for the range of flaw geometries and locations that fall within the implied bounds of Section XI and the explicit bounds of EPRI NP-1181. FAVOR calculates K_I values that are conservatively higher than the 3-D finite-element solutions for embedded flaws located outside of those bounds (specifically, closer to the inner surface than specified by the model limits), but within the region of interest.

1. INTRODUCTION

It has been recognized previously that flaw characterization has the greatest level of uncertainty among the input data required to perform probabilistic fracture mechanics (PFM) analyses of reactor pressure vessels (RPVs) subjected to pressurized-thermal-shock (PTS) loading conditions [1-3]. To reduce that uncertainty, the U. S. Nuclear Regulatory Commission (NRC) is supporting research to establish an improved technical basis for acquiring flaw-characterization data (including the number, location, and size of flaws) for RPV materials. In one such research effort, the Pacific Northwest National Laboratory (PNNL), under contract to the NRC, performed nondestructive and destructive examinations of material taken from the Pressure Vessel Research Users Facility (PVRUF) [4], located at ORNL. While a considerably higher

number of flaws were found in PVRUF vessel than had been postulated previously in the Integrated Pressurized Thermal Shock (IPTS) studies [1-3], all were embedded flaws, i.e., no surface-breaking flaws were detected [4]. Previous studies [5-6] have shown that the first 1/8th of the RPV wall thickness is the most active region for predicting cleavage initiation of embedded flaws. Embedded flaws with the inner crack tip located in the region between 1/8th and 3/8th of the RPV wall thickness are also predicted to initiate, but with a much lower frequency. With this and other improved information, it is anticipated that embedded flaws will play a significant role in future analyses of RPVs subjected to transient loading conditions such as PTS.

The FAVOR computer program [7-8] is currently under development at ORNL to perform Method-2 type of PFM analyses of RPVs subjected to transient loading conditions such as PTS. In the more traditional Method-1 type of PFM analysis, all flaws were postulated to extend to the inner surface. In the Method-2 type of analysis, the postulated flaw population in the RPV can be inner-surface breaking and/or embedded flaws. The Method-2 type of analysis will also include quantification of uncertainty regarding flaw characterization. A considerable effort has been directed previously toward validating the K_I solutions generated by FAVOR for inner-surface breaking flaws [9]. Since embedded flaws will play a significant role in future PFM analyses, it is important that the computational fracture mechanics model implemented into FAVOR for embedded flaws also be "benchmarked."[1] The FAVOR methodology for calculating K_I factors for embedded flaws is the EPRI NP-1181 analytical interpretation [10] of the ASME Section XI-Appendix A [11] for embedded flaws. In Subarticle IWB-3610 of ASME Section XI, the class of subsurface flaws can include flaws that lie in both the ferritic steel base and cladding ("in-clad"), flaws that lie entirely in the ferritic steel base but terminate at the clad/base interface ("subclad"), and flaws that are contained entirely within the base material ("embedded"). Only the subclass of "embedded" subsurface flaws are investigated in this study.

This report describes the benchmarking study that was performed to compare K_I factors computed by FAVOR for planar embedded-flaws to solutions obtained from two independently developed computer models. Specifically, calculations for a matrix of planar embedded flaws generated with FAVOR are compared with those from the two following sources:

- Separate computer code (SUBCOR) developed at ORNL for this study that uses the same EPRI NP-1181 parametric equations to provide a benchmark check; and

---

[1] In the nomenclature of software quality assurance procedures, "benchmarking" involves code-to-code comparisons; "verification" involves comparisons of code results to closed-form solutions; and "validation" involves comparisons of code results to experimental data.

- three-dimensional finite-element models of the embedded flaw matrix analyzed using the ABAQUS computer program [12] to provide an independent check of both the ASME subsurface flaw model and the FAVOR implementation.

Results and conclusions drawn from these comparative assessments are described in the following sections.

2. FAVOR COMPUTER PROGRAM

The FAVOR computer program uses the finite-element method to generate one-dimensional thermal and stress distributions (circumferential and axial) through the wall thickness of a clad RPV subjected to complex time-varying thermal-hydraulic boundary conditions. FAVOR employs stress intensity factor influence coefficients (SIFICs) and superposition techniques to calculate time-dependent values of K_I for various flaw geometries that penetrate the inner surface. A database of SIFICs has been generated for (1) infinite-length axial flaws, (2) continuous 360-degree circumferential flaws, and (3) axially and circumferentially-oriented finite-length semielliptical inner surface flaws with aspect ratios of 2, 6, and 10 [13-15]. This database has been implemented into the FAVOR code. FAVOR has been validated to generate thermal, stress, and K_I solutions for inner surface-breaking flaws that are within 1-2 percent of ABAQUS 3-dimensional finite-element benchmark solutions [9]. ABAQUS is a nuclear quality assurance certified (NQA-1), general-purpose, multidimensional finite-element code that has fracture mechanics capabilities. The version of FAVOR currently under development will have the capability to analyze an RPV that has a combination of inner-surface breaking flaws and/or subsurface (embedded) flaws. One of the main objectives of this study is to check the implementation of the FAVOR methodology to calculate K_I factors for embedded flaws.

For embedded flaws, the FAVOR code utilizes the EPRI analytical representation [10] of the ASME Code elliptical subsurface flaw model [11]. Article A-3000 in Section XI, Appendix A of the ASME code recommends a procedure for the calculation of the Mode I K_I factor based on the resolution of nonlinear applied stresses into the linear superposition of approximate membrane and bending components. Those components are described by equivalent linear representations through the thickness of the wall. Thus, Mode I K_I factor is computed from the following relation:

$$K_I = (M_m \sigma_m + M_b \sigma_b)\sqrt{\pi a / Q} \quad , \qquad (1)$$

where

a = the minor axis of the elliptical subsurface flaw

Q = flaw shape parameter

M_m = free-surface correction factor for membrane stresses

M_b = free-surface correction factor for bending stresses

σ_m = membrane stress

σ_b = bending stress

Figure 1 presents a schematic of the ASME subsurface flaw model including the relevant descriptive variables and aspect ratios. Section XI, Article A-3000 provides the curves shown in Figs. 2 and 3 for the variables M_m and M_b in Eq. (1). An approximate equation for the flaw shape parameter, Q, is given in Ref. 11 with the form

$$Q = 1 + 4.593\left(a/l\right)^{1.65} - q_y \quad , \qquad (2)$$

where $2a$ is length of the minor axis, l is the length of the major axis, and q_y is the plastic-zone correction factor. The correction factors for M_m and M_b are provided for the inner (Point 1) and outer (Point 2) extremes of the minor diameter ($2a$) of the embedded elliptical flaw. Parametric equations for Q, M_m, and M_b were derived in the EPRI study [10] using a combination of analytical and curve-fitting techniques. Those EPRI equations, given in the appendix of Ref. 10, were implemented in the Method-2 version of the FAVOR program, with one exception. Currently, the FAVOR implementation of the Q function does not include the plasticity correction factor, q_y, to the crack size (based on the ratio of the gross tensile stress to the yield stress) that was included in Refs. 10 and 11. Estimates of the maximum numerical errors for the EPRI equations are also provided in the appendix of Ref. 10. For M_m and M_b, errors were typically less than 4 percent, and for Q the estimate was 0.23 percent relative to the original solutions for these parameters.

The stress-linearization procedure depicted in Fig. 4 for a concave upward nonlinear stress profile involves the interpolation of the applied hoop stresses at two points on the flaw crack front, Point 1 at a distance x_1 from the inner surface and Point 2 at a distance x_2 from the inner surface. A straight line is fitted through these two points which represents a linear approximation, $\sigma^*(x)$, of the original nonlinear stress profile, $\sigma(x)$, where x is the distance from the inner surface. The effective membrane stress, σ_m , is located at $x = t/2$ along this line and the

bending stress, σ_b, is the stress at the inner surface (x = 0) minus the membrane stress.

$$\sigma_m = \sigma^*(t/2) = \frac{\sigma(x_2) - \sigma(x_1)}{2a}\left(t/2 - x_1\right) + \sigma(x_1) \tag{3}$$

$$\sigma_b = \sigma^*(0) - \sigma_m = \frac{\sigma(x_1) - \sigma(x_2)}{2a}\left(t/2\right) \tag{4}$$

3. VESSEL MODEL AND MATERIAL PROPERTIES

The representative RPV specified for the study has an inside radius of 2286 mm (90 in.), wall thickness, t, of 228.6 mm (9 in.), and clad thickness of 6.35 mm (0.25 in.) (see Fig. 1). The embedded flaw selected for the study is also shown in Fig. 1. This flaw has an elliptical geometry with minor and major axis dimensions defined by the parameters $2a$ and l, respectively. The inner tip of the flaw is located a distance c from the clad/base interface, and the major axis is located a distance e from the centerline (t/2) of the wall.

The isothermal thermo-mechanical properties used in this study for the base and cladding materials are given in Table 1.

A representative 3-dimensional finite-element model of a 180-degree segment of an RPV shell wall section containing an embedded flaw is depicted in Fig. 5. Finite-element models were constructed using 20-node isoparametric brick elements for the main structure. Collapsed prism elements were employed at the crack tip to produce an appropriate singularity for LEFM analyses. Internal pressure loading was applied to the inner surface of the clad layer. Symmetry-plane boundary conditions were applied to the coordinate planes of the model (excluding the flaw face). A modified version of the ORNL/ORMGEN finite-element mesh generator program [16] was used to generate the models.

An initial study was carried out to determine the minimum shell length and mesh refinement required to produce model-independent linear-elastic solutions for the temperature, stress, and J-integral distributions. For each flaw geometry, the mesh refinement and axial length of the finite-element model were increased independently until stable J-integral distributions were calculated around the embedded flaw for the duration of the transient. Furthermore, temperature and hoop-stress distributions (the latter obtained from an uncracked model) at selected times in the transient were compared with the corresponding FAVOR results to check consistency of the ABAQUS models with those of FAVOR.

Linear heat conduction and linear thermo-elastic constitutive models available in the ABAQUS finite-element code were used in the analysis of the model. The *J*-integral formulation in ABAQUS was employed to generate K_I versus time histories at nodal points around the crack tip; conversion of *J*-to-*K* was based on the plane-strain relation

$$K_I = \sqrt{\frac{E\,J}{(1-\nu^2)}} \quad , \tag{5}$$

where E is Young's modulus and ν is Poisson's ratio.

4. LOADING CONDITIONS

The thermal transient definition is one that was used in the NRC/Electric Power Research Institute (EPRI) co-sponsored PTS benchmarking exercise [17], which is characterized by a stylized exponentially decaying coolant temperature. The following formulation is used for the exponentially decaying thermal transient:

$$T(t) = T_f + (T_i - T_f)\exp(-\beta\, t) \quad , \tag{6}$$

where

$T(t)$ = coolant temperature at time t
T_i = coolant temperature at time $t = 0$
T_f = final coolant temperature
β = exponential decay constant

The final coolant temperature was 65.56 °C (150 °F), and the exponential decay constant, β, was 0.15 min^{-1}. The initial coolant temperature was 287.78 °C (550 °F). The pressure is constant and equal to 6.89 MPa (1 ksi). The axial stress induced in the vessel wall by the internal pressure loading was not included in this analysis. The initial vessel temperature was set at a uniform 287.78 °C (550 °F) through the vessel wall. The convection heat transfer coefficient at the inner surface of the RPV was set to a constant value of 5678.27 W/m^2-K (1000 Btu/h-ft^2-°F); the outer surface was assumed to be adiabatic.

Figure 6 depicts temperature profiles through the RPV wall at selected times in the transient, computed by the ABAQUS code for the finite-element model in Fig. 6 using the initial/boundary conditions defined above. These temperature profiles are in close agreement with solutions generated by FAVOR as shown in Fig. 7.

5. ANALYSIS MATRIX

The development version of FAVOR that performs a Method-2 type of PFM analysis has been designed to read flaw characterization files in a format consistent with output files generated by the RR-PRODIGAL computer code [18]. The RR-PRODIGAL code is an expert-based system developed to predict flaw densities and flaw sizes, as well as the distribution of flaw locations within the RPV wall. RR-PRODIGAL assigns a flaw to one of five categories, defined in terms of the location of the flaw inner crack tip relative to the wetted RPV inner surface.

Category 1 - inner surface-breaking flaws;

Categories 2-5 are embedded flaws with inner crack tip locations as follows:

Category 2 - $t_{clad} < x_1 < t/8$

Category 3 - $t/8 < x_1 < 3t/8$

Category 4 - $3t/8 < x_1 < t/2$

Category 5 - $t/2 < x_1 < t$

In the above, t is the RPV wall thickness, t_{clad} is the thickness of the clad layer, and x_1 is the distance of Point 1 on the flaw from the inner surface of the vessel (see Fig. 1). Each flaw characterization file consists of a 100 x 5 array where the (***i, j***) entry is the flaw density for flaws of category ***j*** that have a through-wall depth of (***i***/100)*t, where t is the RPV wall thickness. The inner tip of an embedded flaw of category ***j*** has equal probability of residing at any location in the interval defined for that flaw category. For example, the inner tip of a Category 2 flaw has equal probability of residing at any location between the clad-base interface and t / 8.

For this study, an analysis matrix was defined that emphasizes Category 2, 3, and 4 embedded flaws. The matrix includes three series of flaws (for a total of nine cases) located in the region of interest. The geometric parameters describing the flaw geometry and location are given in Table 2, and mesh layouts of all nine embedded flaws in Table 2 are presented in Fig. 8. Part of the strategy in defining the matrix was to investigate the K_I versus time history for the largest embedded flaw size found during the destructive examination of the RPV described in Ref. 4. Secondly, the sensitivity of K_I to the inner crack tip location was studied for specified flaw sizes.

A third objective is to illustrate that Category 4 and 5 flaws, as defined above, are benign in PFM assessments of RPVs subjected to severe overcooling transients. They are benign because the

maximum K_I for the largest anticipated flaw size is less than the minimum value of K_{Ic} that could ever be predicted. The lowest predicted K_{Ic} is the –3 σ value on the lower shelf (approximately 28 MPa-√m). The maximum value of K_I generated for case C3, which is a Category 4 flaw, is approximately 14 MPa-√m. Thus, that flaw would never be predicted to initiate in cleavage fracture. Even for a 2 in.-deep flaw with its inner crack tip at the same location, the maximum value of K_I is approximately 20 MPa-√m. Since Category 4 and 5 flaws will never be predicted to initiate during an overcooling event, they did not have to be included in PFM analyses. Exclusion of such non-initiating flaws saves considerable computational time during PFM analyses.

Figure 9 depicts the crack-tip region of the Series A flaws generated for the analysis of an embedded flaw with dimensions of $2a$ = 17 mm and l = 102 mm. The only geometric variable within each series of flaws is the distance, *c,* from the inner-most point of the flaw (Point 1 in Fig. 1) to the clad/base interface. The minor axis dimension of 17 mm (0.67 in.) corresponds to the largest flaw found in the destructive examination in Ref. 1. The analysis matrix also includes embedded flaws with smaller (Series B) and larger (Series C) minor axis dimensions. Series B also has a different major to minor axis aspect ratio than Series A and C. The crack-tip regions for Series B and C are shown in Figs. 10 and 11, respectively.

In the acceptance criteria of subsection IWB-3610 of the ASME Code, a proximity rule is given in Fig. IWB-3610-1 to delineate the transition from a subsurface flaw to a surface flaw. Using the nomenclature of Fig. 1, if the ratio (x_1/a) is less than 0.4, then "in-clad," "subclad," and "embedded" flaws are treated as surface-breaking flaws for the purposes of analysis by the flaw model presented in Ref. 11. For all of the embedded flaws in the analysis matrix, the ratio (x_1/a) is greater than 0.4 and, therefore, they are all considered subsurface flaws by the ASME code.

6. RESULTS AND DISCUSSION

6.1 Benchmarking of EPRI Flaw Model Implementation into FAVOR

A separate computer code (SUBCOR) was developed to establish a benchmark calculation for the FAVOR implementation of the EPRI subsurface flaw model [10]. SUBCOR uses the parametric equations for model parameters Q, M_m, and M_b from Ref. 10, along with hoop stress profiles generated by ABAQUS (with no flaw present in the vessel wall), to calculate applied K_I histories for Point 1 on the embedded flaw (see Fig. 1). A listing of the subroutines that calculate these flaw model parameters in the benchmarking code is given in the Appendix. In Fig. 12, hoop stress profiles calculated by FAVOR and ABAQUS at 10 and 16 min. into the PTS transient are compared. The effect of the differences between the FAVOR and ABAQUS hoop-stress

solutions near the clad/base interface will be discussed in the results section for Case A1.

The subroutine *Qflaw* (listed in the Appendix) calculates three values for the Q parameter. The first form of Q is its formal definition based on the complete elliptic integral of the second kind, $E(x)$,

$$
\begin{aligned}
&Q(x) = E^2(x) \\
&E(x) = \int_0^{\pi/2} \sqrt{\left(1 - x\sin^2(\theta)\right)}\, d\theta \text{ for } 0 \le x \le 1 \\
&x = 1 - 4(a/l)^2
\end{aligned}
\tag{7}
$$

In Ref. 10, the elliptic integral is replaced by an infinite series approximation for Q,

$$
\begin{aligned}
&Q \approx \frac{\pi^2}{4(1+m)^2}\left[1 + \frac{m^2}{4} + \frac{m^4}{64} + \frac{m^6}{256} + \left(\frac{5}{128}\right)^2 m^8 + \left(\frac{7}{256}\right)^2 m^{10}\right]^2 \\
&m = \frac{1 - 2(a/l)}{1 + 2(a/l)}
\end{aligned}
\tag{8}
$$

A simpler equation for an estimate of the flaw shape parameter, Q, is given in Ref. 11 with the form (omitting the plastic zone correction factor, q_y)

$$
Q = 1 + 4.593\left(a/l\right)^{1.65} \quad . \tag{9}
$$

The elliptic integral of the second kind in Eq. (7) is available in the IMSL Special Functions Library [19] and was applied in the benchmark code developed for this study. For the embedded flaws in the analysis matrix, all three equations were used to calculate the Q parameter and Eqs. (8) and (9) were found to agree with Eq. (7) to within a maximum relative deviation of 0.05 percent.

As reported in Ref. 10, the original source for the M_m curves in Fig. 2 was the report by Wilhelm [20] published in 1970 based on the work of Kobayashi, et al., [21] in 1965, and the results for M_b in Fig. 3 were originally published by Shah and Kobayashi [22] in 1972. The parametric equations given in Ref. 10 take the form of polynomial curve fits with the aspect ratios $2e/t$ and $2a/t$ as arguments. See the subroutines in the Appendix for the details of these parametric equations.

In Figure 13, the values of M_m for the nine flaws in the analysis matrix are plotted as a function of the eccentricity aspect ratio $2e/t$. Parametric curves for three aspect ratios, i.e., $2a/t = 0.08$ (flaw A), 0.01 (flaw B) and 0.11 (flaw C), are also plotted in Fig. 13. In Fig. 2, the implied flaw eccentricity ratio bounds are $0 \leq 2e/t \leq 0.6$ for corresponding aspect ratio bounds of $0.15 \leq 2a/t \leq 0.45$; however, in Ref. 10, explicit bounds for the parametric equations for M_m are not given. As can be observed in Fig. 13, only two of the embedded flaws (Cases A4 and C3) are within the eccentricity ratio bounds of Fig. 2, and all nine flaws are below the lower bound of 0.15 for aspect ratio $2a/t$.

Figure 14 plots the values of M_b for the nine flaws in the analysis matrix as a function of the eccentricity aspect ratio $2e/t$. Parametric curves for the flaw aspect ratio, $2a/t$, corresponding to flaws A, B and C, are also plotted in Fig. 14. Figure 3 provides M_b curves for Point 1 that are bounded by $0 \leq 2e/t \leq 0.7$ for aspect ratio bounds of $0.1 \leq 2a/t \leq 0.3$. The explicit bounds stated in Ref. 10 for the Point 1 M_b curves are $0 \leq 2e/t \leq 0.7$ for aspect ratios satisfying $0.1 \leq 2a/t \leq 0.7$. In the analysis matrix, only the three flaws in Series C satisfy the lower bound of the $2a/t$ aspect ratio (i.e., $2a/t \geq 0.1$), and five flaws (Cases A3, A4, B2, C2, and C3) satisfy the eccentricity ratio upper bound of 0.7. As shown in Fig. 14, as the eccentricity ratio exceeds its upper bound of 0.7, the EPRI curve fits for M_b begin to rapidly increase with very high slopes near $2e/t \approx 0.9$.

In comparing the FAVOR solutions with the benchmark code SUBCOR results, all flaws in the analysis matrix produced close agreement, except for Case A1. Comparative results for Series A (i.e., A2, A3 and A4) are shown in Fig. 15, Series B in Fig. 16 and Series C in Fig. 17. For Case A1 (Fig. 18), the maximum deviation between FAVOR and SUBCOR occurred at 16 min. into the PTS transient; the benchmark code (designated SUBCOR(ABAQUS $\sigma_{\theta\theta}$) produced a K_I approximately 4.4 percent higher than the FAVOR solution. In checking these results, it was determined that FAVOR and SUBCOR(ABAQUS $\sigma_{\theta\theta}$) were calculating essentially identical values of Q, M_m, and M_b; however, the differences in the hoop stress profiles calculated by FAVOR and ABAQUS near the clad/base interface (see Fig. 12) produced a difference in the stress linearization approximation as shown in Fig. 19. By repeating the PTS transient using the FAVOR hoop stresses, the benchmark code (designated SUBCOR(FAVOR $\sigma_{\theta\theta}$) in Fig. 19) produced a peak K_I that was within 0.8 percent of the value calculated by FAVOR. Case A1 is a small Category 2 embedded flaw ($2a/t = 0.074$) that is very close to the clad/base interface ($c = 1.9$ mm and $2e/t = 0.853$). As a result of its geometry and location, the applied K_I calculated by the EPRI model for A1 is very sensitive to approximation errors associated with the linearization of the rapidly changing hoop stress gradient near the clad/base interface.

6.2 Benchmarking of FAVOR with ABAQUS 3-D Finite-Element Solutions

Profiles of the *J*-integrals calculated by the ABAQUS code for all nine flaws in the analysis matrix are plotted in Fig. 20. These profiles were taken from the times in the PTS transient at which the maximum K_I-values occurred at Point 1 [see Fig. 20 (d)] on the flaw front. As expected, the crack driving force around the flaw front at a fixed time is a maximum at Point 1; it decreases monotonically as the distance between Point 1 and the clad interface, c, is increased.

The K_I versus time solutions generated with FAVOR and ABAQUS for all flaws in the analysis matrix are compared in Figs. 21-24. Values of K_I at 16 min are compared in Table 3; solutions at peak K_I are compared in Table 4. There was close agreement between the solutions for all but one case, i.e., Case A1. These comparisons are shown for Series A (A2, A3and A4) in Fig. 21, Series B in Fig. 22 and Series C in Fig. 23. For Case A1 in Fig. 24, the maximum value of K_I from FAVOR is approximately 20 percent higher than that calculated from the ABAQUS 3-D finite-element model. It was noted in the previous section that Case A1 is very close to the clad/base interface, where the applied K_I from the EPRI mode is very sensitive to approximation errors due to linearization of the non-linear stress gradient near the clad/base interface.

7. CONCLUSIONS

A set of K_I versus time solutions were generated for a matrix of subsurface flaw geometries embedded in an RPV wall subjected to transient PTS loading conditions. Solutions from a development version of the FAVOR code that incorporates the EPRI analytical interpretation of the ASME Section XI-Appendix A methodology were compared with those obtained from two independently developed computer models. Those comparisons were used to evaluate the ASME model, as implemented in FAVOR, for fracture assessment of embedded flaws. Results for the analysis matrix showed that FAVOR calculates applied K_I solutions for embedded flaws that agree closely with the two independent benchmark solutions for the range of flaw geometries and locations that fall within the implied bounds of Section XI and the explicit bounds of EPRI NP-1181. For flaws in the analysis matrix outside of those bounds (specifically, closer to the inner surface than specified by the model limits) but within the region of interest, FAVOR calculated K_I values that are conservatively higher than the 3-D finite-element solutions.

References

1. T. J. Burns et al., *Preliminary Development of an Integrated Approach to the Evaluation of Pressurized- Thermal-Shock as Applied to the Oconee Unit 1 Nuclear Power Plant,* NUREG/CR-3770 (ORNL/TM-9176), Oak Ridge National Laboratory, May 1986.

2. D. L. Selby et al., *Pressurized-Thermal-Shock Evaluation of the Calvert Cliffs Unit 1 Nuclear Power Plant,* NUREG/CR-4022 (ORNL/TM-9408), Oak Ridge National Laboratory, September 1985.

3. D. L. Selby et al., *Pressurized-Thermal-Shock Evaluation of the H.B. Robinson Nuclear Power Plant,* NUREG/CR-4183 (ORNL/TM-9567), Oak Ridge National Laboratory, September 1985.

4. G. J. Schuster, S. R. Doctor, and P. G. Heasler, *Characterization of Flaws in U.S. Reactor Pressure Vessels: Density and Distribution of Flaw Indications in PVRUF,* NUREG/CR-6471, Vol. 1 (PNNL-11143) Pacific Northwest National Laboratory, November 1998.

5. T. L. Dickson and F. A. Simonen, "Inclusion of Embedded Flaws in Pressurized Thermal Shock Analyses of Nuclear Reactor Pressure Vessels," PVP-Vol. 46, *Fatigue and Fracture,* ASME 1997.

6. T. L. Dickson et al., "Revisiting the Integrated Pressurized Thermal Shock Studies of an Aging Pressurized Water Reactor," *Fracture Design Analysis of Pressure Vessels, Heat Exchangers, Piping Components, and Fitness for Service*, PVP-Vol. 388, pp. 79-89, ASME, 1999.

7. T. L. Dickson, *FAVOR: A Fracture Analysis Code for Nuclear Reactor Pressure Vessels, Release 9401,* ORNL/NRC/LTR 94-1, Oak Ridge National Laboratory, February 1994.

8. T. L. Dickson, "An Overview of FAVOR: A Fracture Analysis Code for Nuclear Reactor Pressure Vessels," *Transactions of the 13th International Conference on Structural Mechanics in Reactor Technology (SMiRT 13),* Volume IV, pp. 701-706, Porto Alegre, Brazil, August, 1995.

9. T. L. Dickson, "Validation of FAVOR Code Linear Elastic Fracture Solutions for Finite-Length Flaw Geometries," PVP-Vol. 304, *Fatigue and Fracture Mechanics in Pressure Vessels and Piping*, ASME, 1995.

10. *Computational Method to Perform the Flaw Evaluation Procedure as Specified in the ASME Code, Section XI, Appendix A, Part 1: General Description and Background*, EPRI NP-1181, Failure Analysis Associates, Palo Alto, CA, September 1979.

11. *American Society of Mechanical Engineers Boiler and Pressure Vessel Code,* Section XI, Rules for Inservice Inspection of Nuclear Power Plant Components, Appendix A, Analysis of Flaws, Article A-3000, Method for K_I Determination, American Society of Mechanical Engineers, New York, 1998.

12. *ABAQUS Theory Manual,* Version 5.8, Hibbitt, Karlson, and Sorenson, Inc., Providence, Rhode Island, 1998

13 J. W. Bryson and T. L. Dickson, "Stress Intensity Factor Influence Coefficients for Axial and Circumferential Flaws in Reactor Pressure Vessels," *Pressure Vessel Integrity,* PVP Vol. 250, pp. 77-88, ASME, 1993.

14. J. A. Keeney and T. L. Dickson, *Stress-Intensity-Factor Influence Coefficients for Axially Oriented Semielliptical Inner-Surface Flaws in Clad Vessels (R_i/t = 10),* ORNL/NRC/LTR-93/33, Revision 1, Oak Ridge National Laboratory, September 1995.

15. J. W. Bryson and T. L. Dickson, *Stress-Intensity-Factor Influence Coefficients for Circumferentially Oriented Semielliptical Inner-Surface Flaws in Clad Vessels (R_i/t = 10),* ORNL/NRC/LTR-94/8, Oak Ridge National Laboratory, April 1994.

16. B. R. Bass and J. W. Bryson, *Application of Energy Release Rate Techniques to Part-Through Cracks in Plates and Cylinder, Volume 1, ORMGEN-3D: A Finite-Element Mesh Generator for 3-Dimensional Crack Geometries,* NUREG/CR-2997 Vol. 1 (ORNL/TM-8527/V1), Oak Ridge National Laboratory, December 1982.

17. B. A. Bishop, *Benchmarking of Probabilistic Fracture Mechanics Analyses of Reactor Vessels Subjected to Pressurized Thermal Shock Loading*, EPRI Research Project 2975-5*,* 1993.

18. O. J. V. Chapman and F. A. Simonen, *RR-PRODIGAL - A Model for Estimating the Probabilities of Defects in Reactor Pressure Vessel Welds*, NUREG/CR-5505, Pacific Northwest National Laboratory, October 1998.

19. *IMSL Fortran and C Application and Development Tools*, Visual Numerics, Inc., Houston, Texas, 1997.

20. D. P. Wilhelm, *Fracture Mechanics Guideline for Aircraft Structural Applications,* AFDL-TR-69-11, Northrup Corporation, February 1970.

21. A. S. Kobayashi, M. Ziv, and L. R. Hall, "Approximate Stress Intensity Factor for an Embedded Elliptical Crack Near Two Parallel-Free Surfaces," *International Journal of Fracture Mechanics,* **1**, (1965) 81.

22. R. C. Shah and A. S. Kobayashi, "Stress Intensity Factor for an Elliptical Crack Approaching the Surface of a Plate in Bending," ASTM STP 513, (1972) 3.

Table 1. RPV Thermal and Mechanical Properties

Property	Units	Cladding	Base
Thermal conductivity	W/m-K	17.31	41.54
	Btu/h-ft-°F	10.0	24.0
Specific heat	J/kg-K	502.4	502.4
	Btu/lbm-°F	0.12	0.12
Modulus of elasticity	GPa	157.2	193.0
	ksi	22 800	28 000
Poisson's ratio		0.3	0.3
Thermal expansion	K^{-1}	17.01×10^{-6}	13.99×10^{-6}
coefficient	$°F^{-1}$	9.45×10^{-6}	7.77×10^{-6}
Density	kg/m^3	7833	7833
	lbm/ft^3	489	489

Table 2. Embedded Flaw Case Matrix

Case	RR Category	$2a$ (mm)	l (mm)	c (mm)	a (mm)	e (mm)	$l/2a$	$2a/t$	$2e/t$	Q EPRI	Q ASME	M_b EPRI	M_m EPRI
A1	2	17.02	101.6	1.9	8.51	97.5	6	0.074	0.853	1.0770	1.0767	0.9812	1.0367
A2	2	17.02	101.6	8.0	8.51	91.4	6	0.074	0.800	1.0770	1.0767	0.8766	1.0286
A3	3	17.02	101.6	28.6	8.51	70.9	6	0.074	0.620	1.0770	1.0767	0.6658	1.0128
A4	3	17.02	101.6	76.2	8.51	23.2	6	0.074	0.203	1.0770	1.0767	0.2551	1.0039
B1	2	2.54	25.4	2.5	1.27	104.1	10	0.011	0.911	1.0321	1.0328	0.9951	1.0010
B2	3	2.54	25.4	28.6	1.27	78.1	10	0.011	0.683	1.0321	1.0328	0.6961	1.0004
C1	2	25.4	152.4	3.8	12.70	91.4	6	0.111	0.800	1.0764	1.0761	0.9254	1.0651
C2	3	25.4	152.4	25.4	12.70	69.9	6	0.111	0.611	1.0764	1.0761	0.6765	1.0281
C3	4	25.4	152.4	85.7	12.70	9.5	6	0.111	0.083	1.0764	1.0761	0.1479	1.0077

15

Table 3. Comparison of FAVOR and ABAQUS solutions at 16 min.

Case	FAVOR MPa-√m	ABAQUS Plane Strain MPa-√m	Δ*K* MPa-√m	Percent Deviation	ABAQUS Plane Stress MPa-√m	Δ*K* MPa-√m	Percent Deviation
A1	74.64	63.52	11.12	17.51	60.59	14.05	23.18
A2	65.09	64.96	0.13	0.19	61.97	3.12	5.03
A3	45.56	48.44	-2.88	-5.94	46.21	-0.65	-1.40
A4	14.85	13.88	0.96	6.93	13.24	1.60	12.10
B1	29.79	26.57	3.23	12.14	25.34	4.45	17.56
B2	19.05	16.75	2.30	13.73	15.98	3.07	19.22
C1	84.89	86.10	-1.21	-1.41	82.14	2.75	3.35
C2	56.95	56.76	0.19	0.33	54.14	2.80	5.17
C3	10.52	10.00	0.52	5.21	9.54	0.98	10.29

Table 4. Comparison of FAVOR and ABAQUS solutions at peak K_I.

Case	FAVOR MPa-√m	ABAQUS Plane Strain MPa-√m	Δ*K* MPa-√m	Percent Deviation	ABAQUS Plane Stress MPa-√m	Δ*K* MPa-√m	Percent Deviation
A1	74.64	63.52	11.12	17.51	60.59	14.05	23.18
A2	65.10	64.99	0.11	0.16	62.00	3.10	5.00
A3	46.02	48.71	-2.69	-5.52	46.46	-0.44	-0.95
A4	16.56	15.72	0.84	5.35	15.00	1.57	10.44
B1	29.80	26.57	3.24	12.19	25.34	4.46	17.60
B2	19.20	16.96	2.24	13.20	16.18	3.02	18.66
C1	84.89	86.10	-1.21	-1.41	82.14	2.75	3.35
C2	57.45	57.33	0.12	0.21	54.69	2.76	5.05
C3	13.30	12.87	0.43	3.35	12.27	1.02	8.35

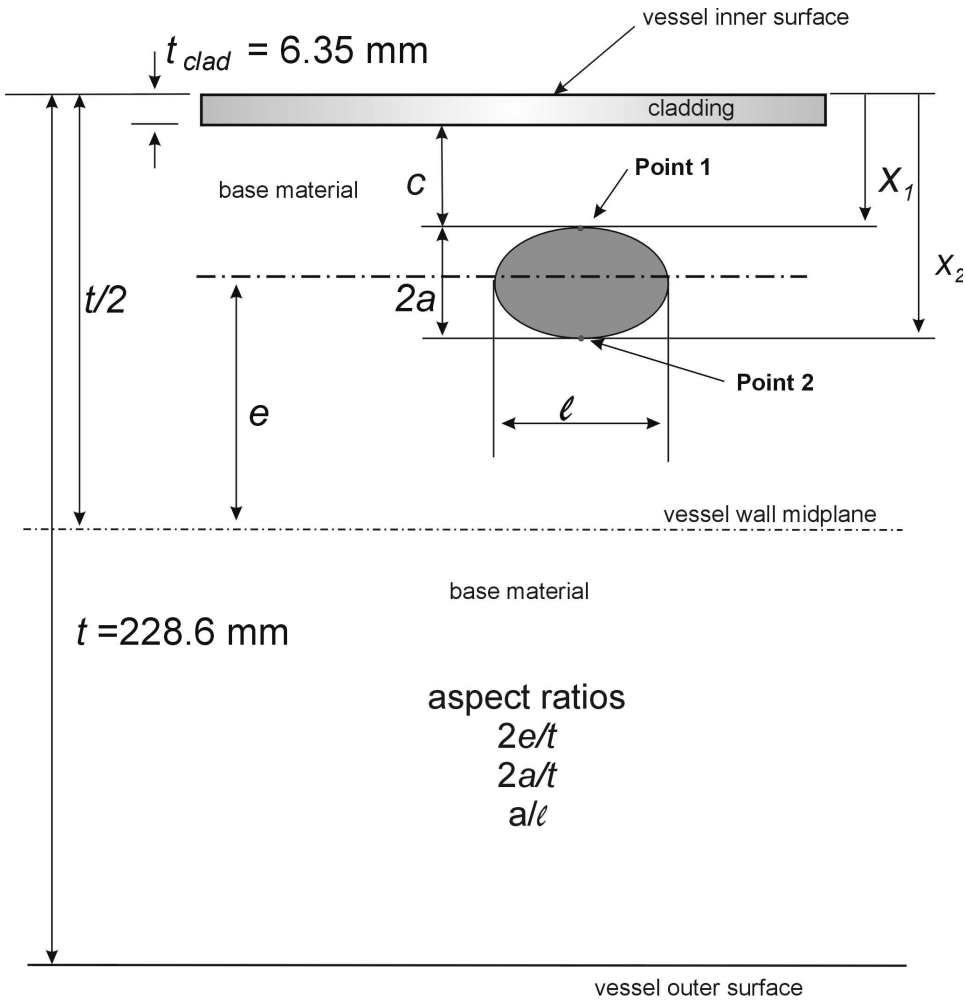

Fig. 1. Geometry and nomenclature used in embedded (subsurface) flaw model.

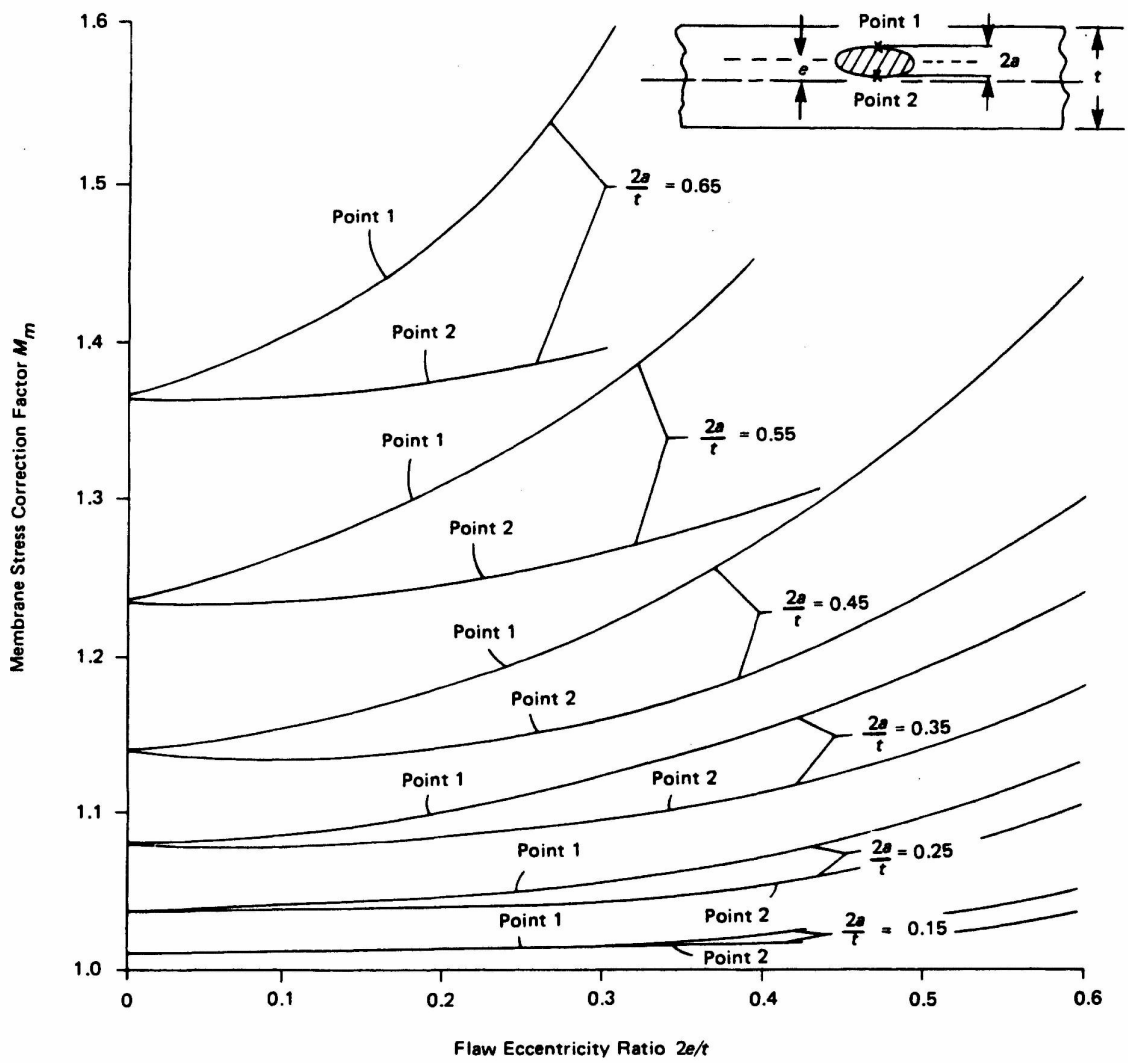

t = wall thickness
e = eccentricity
Point 1 = outer extreme of the minor diameter of ellipse (closer to surface)
Point 2 = inner extreme of the minor diameter of ellipse (further from surface)

Fig. 2. Membrane stress correction factor for subsurface flaws (adapted from Fig. A-3310-1 in Ref. (12)).

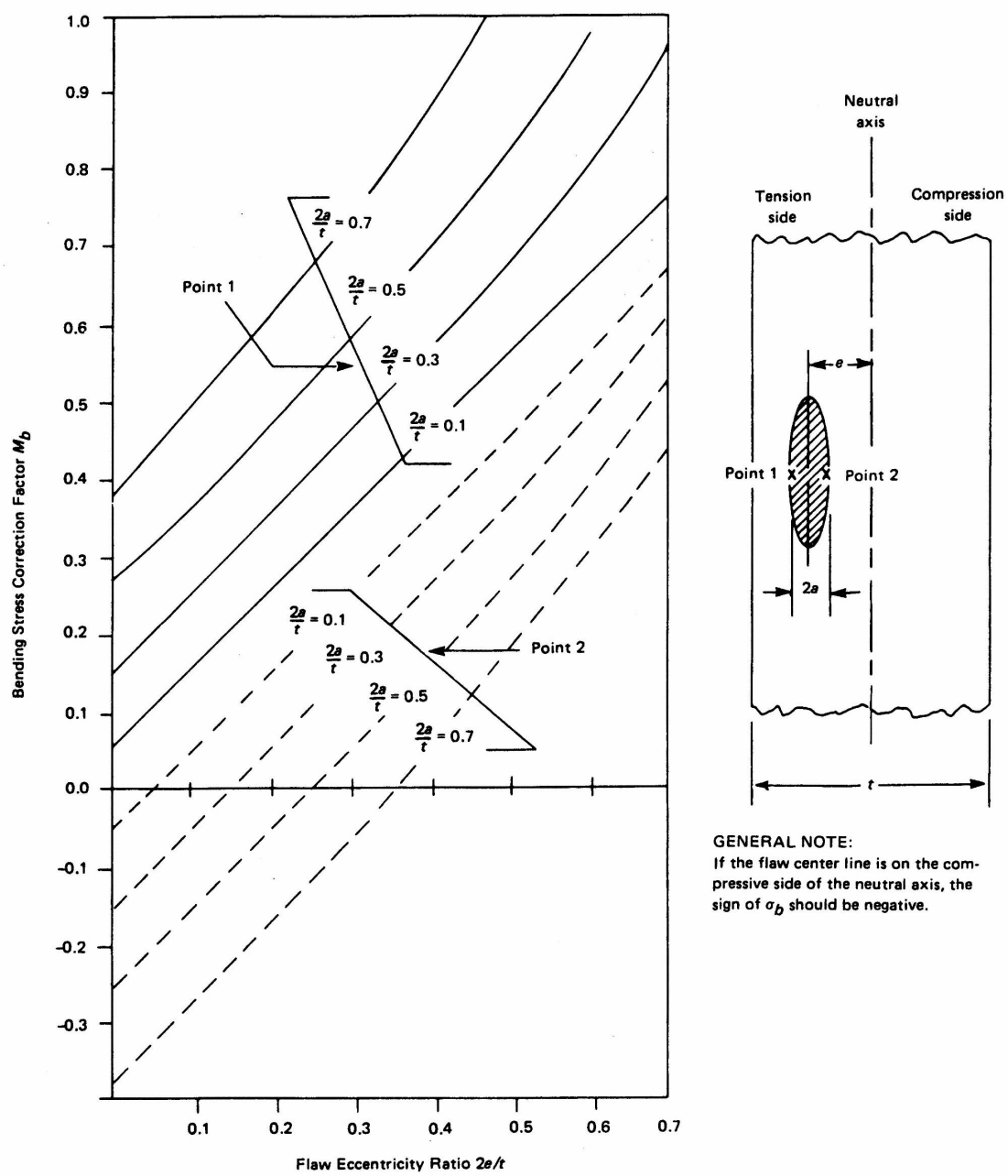

Fig. 3. Bending stress correction factor for subsurface flaws (adapted from Fig. A-3310-2 in Ref. (12))

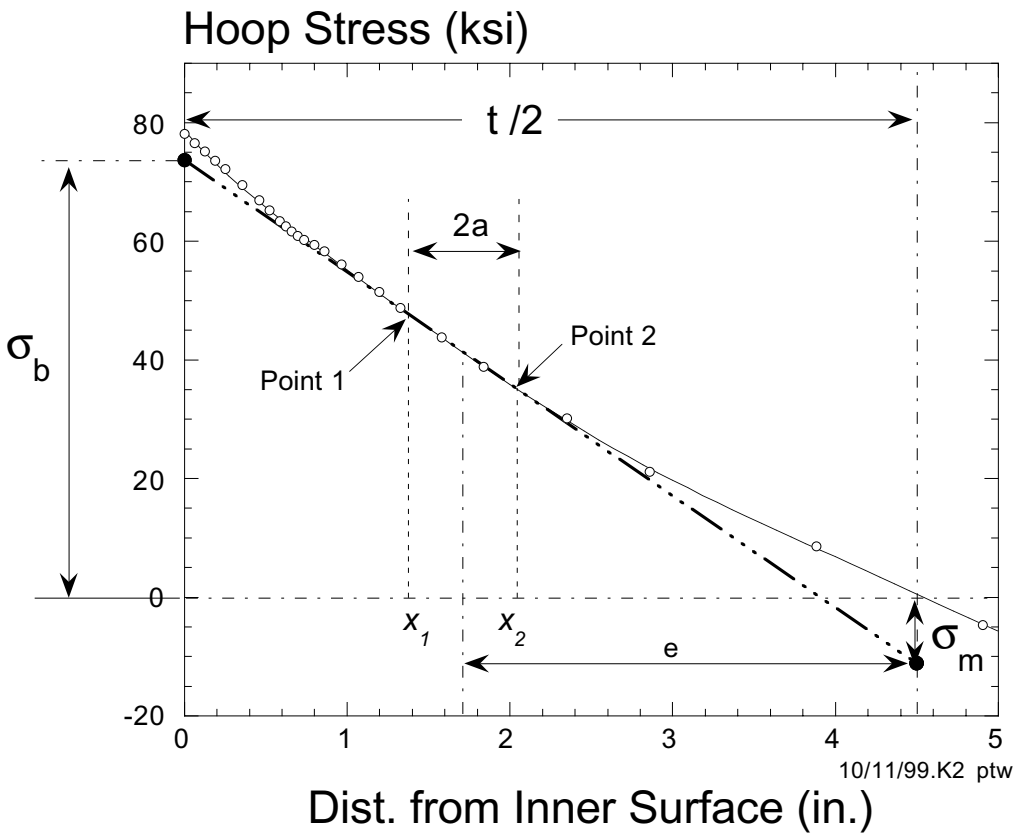

Fig. 4. Resolution of computed nonlinear stress profile into the linear superposition of effective membrane and bending stresses.

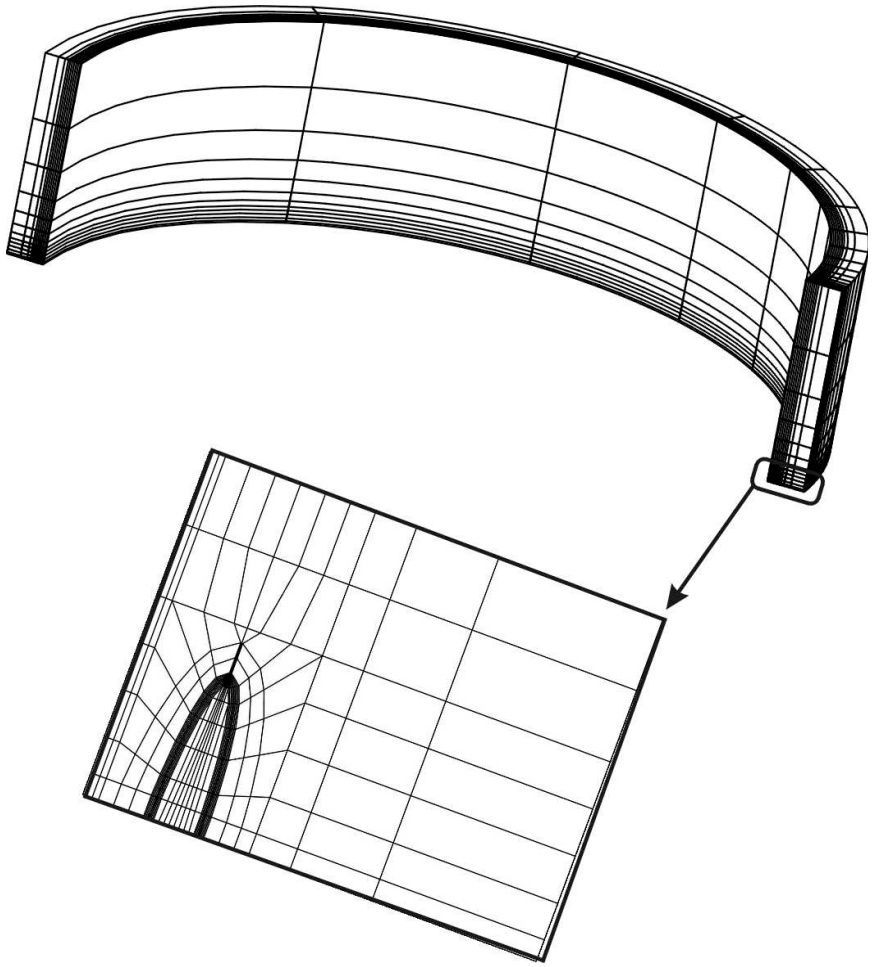

Fig. 5. Finite-element model of RPV with an embedded elliptical flaw.

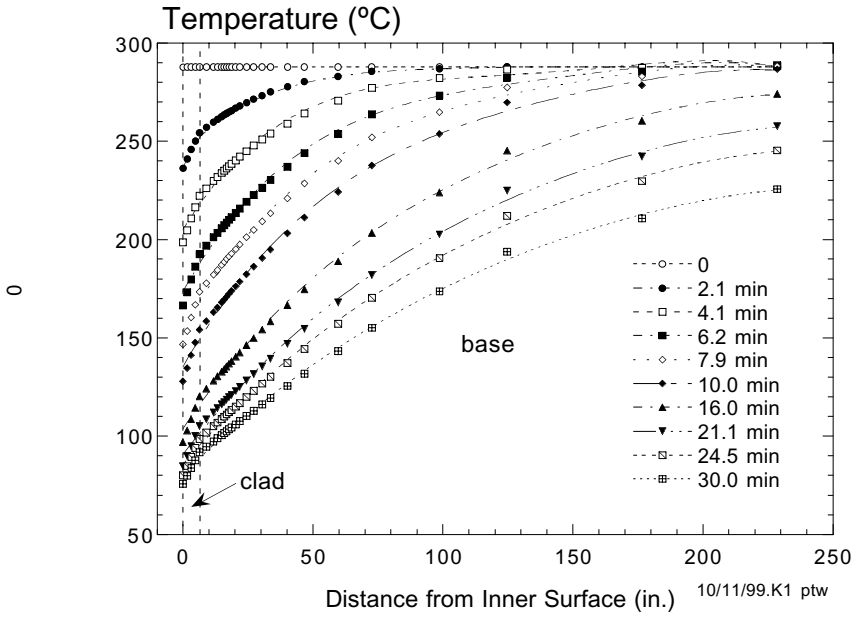

Fig. 6. Temperature profiles through the vessel wall calculated for the PTS transient.

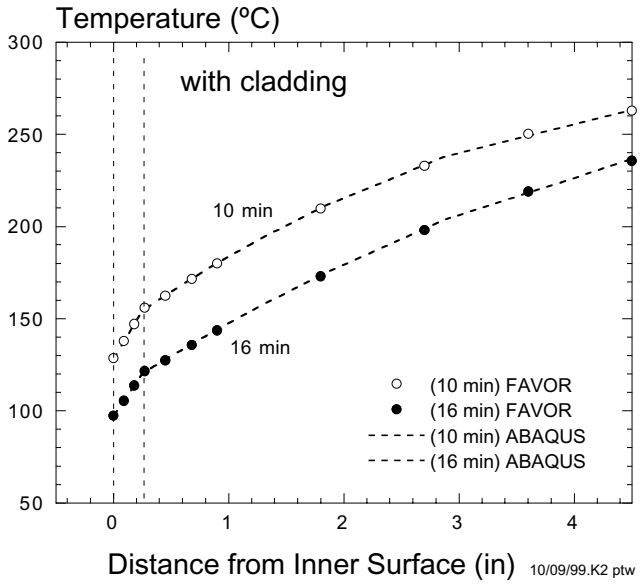

Fig. 7. Comparison of temperature profiles calculated by FAVOR (symbols) and ABAQUS (dashed lines) at 10 and 16 minutes into the PTS transient.

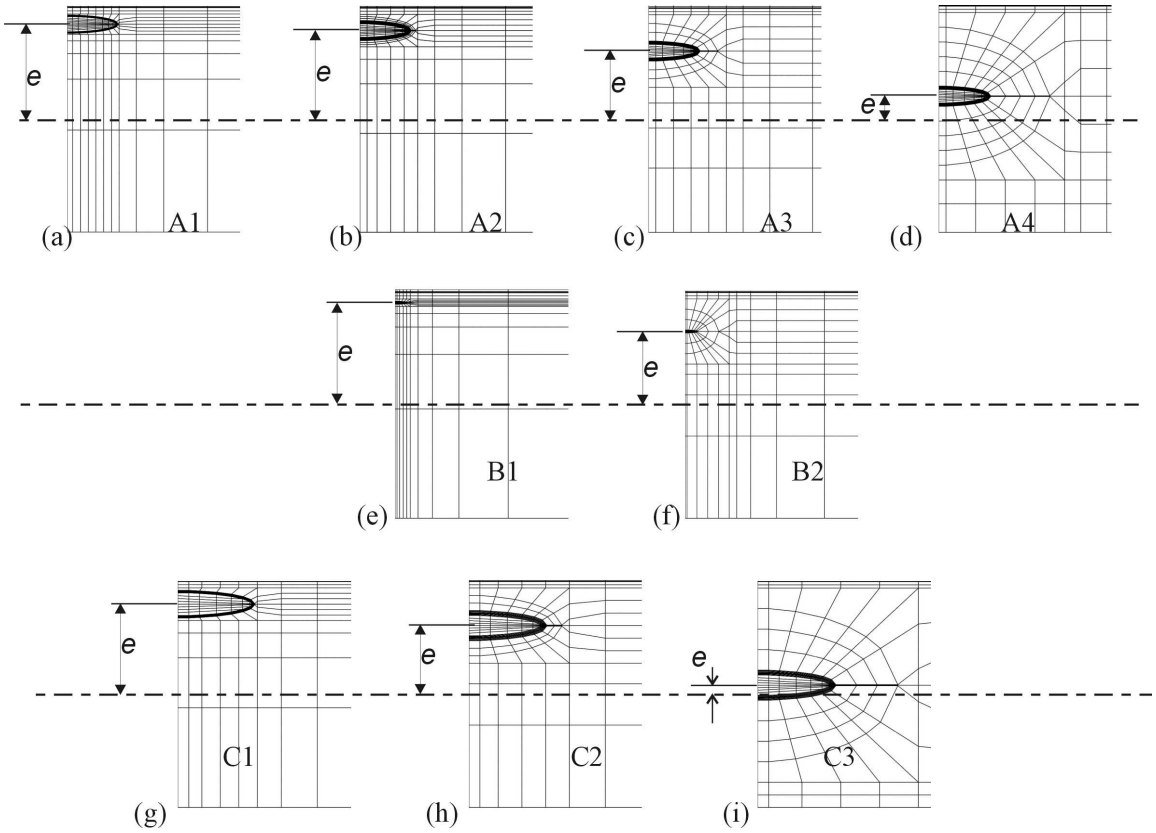

Fig. 8. Mesh layouts of embedded flaw case matrix: Series A, B, and C.

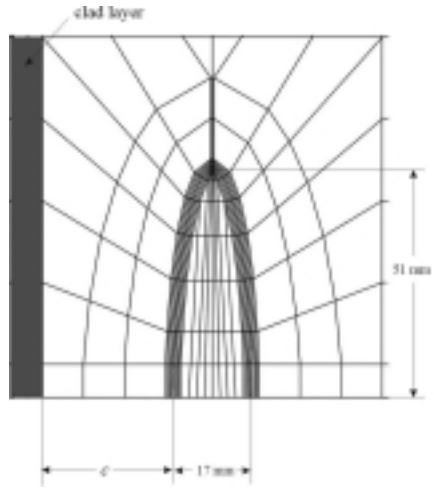

Fig. 9. Series A flaws with 2*a* = 17 mm and l = 102 mm.

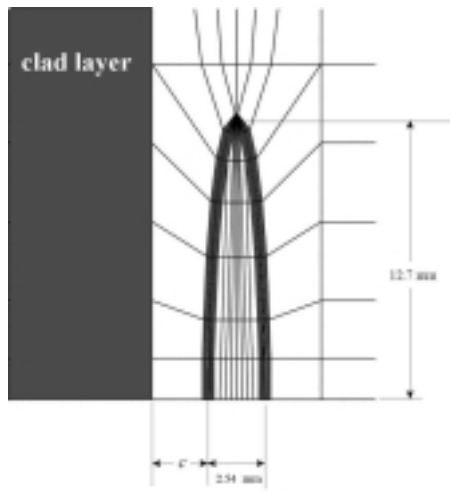

Fig. 10. Series B flaws with 2*a* = 2.54 mm and l = 25.4 mm.

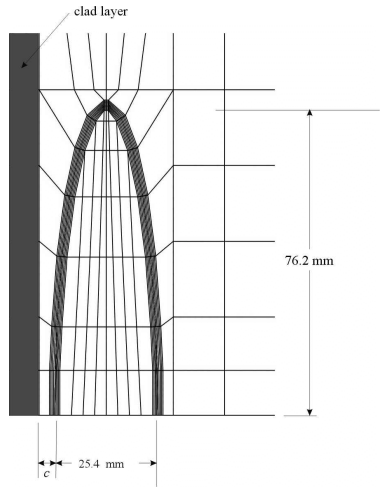

Fig. 11. Series C flaws with 2*a* = 25.4 mm and l = 152.4 mm.

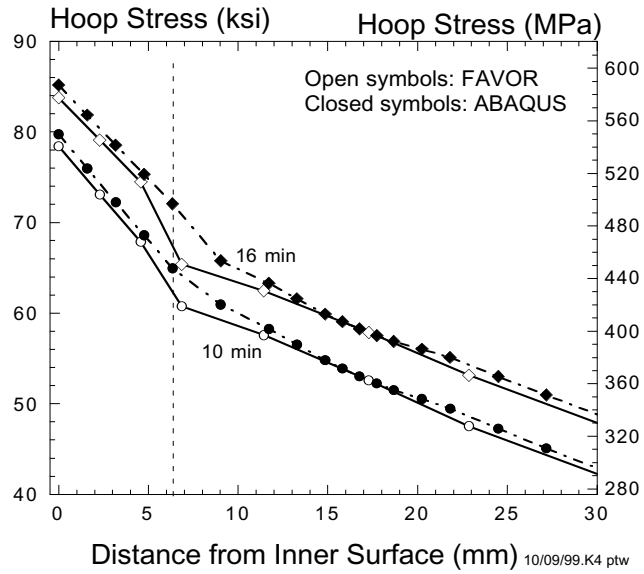

Fig. 12. Comparison of hoop stress profiles calculated by FAVOR and ABAQUS.

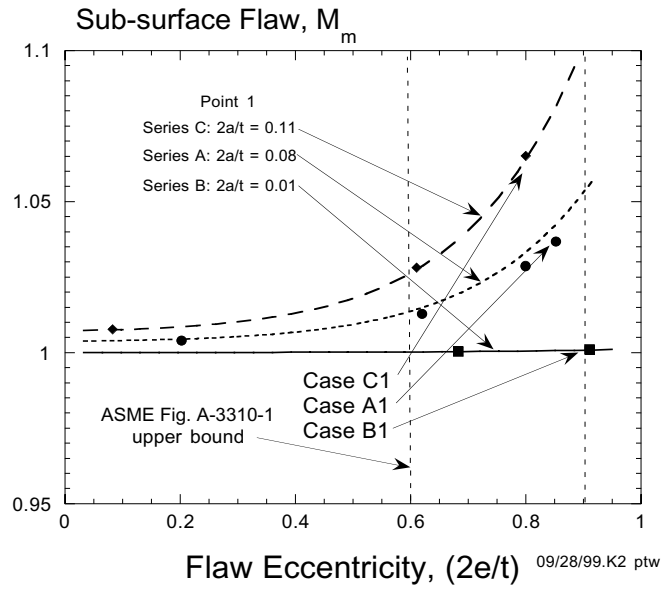

Fig. 13. Membrane stress correction factors for analysis matrix.

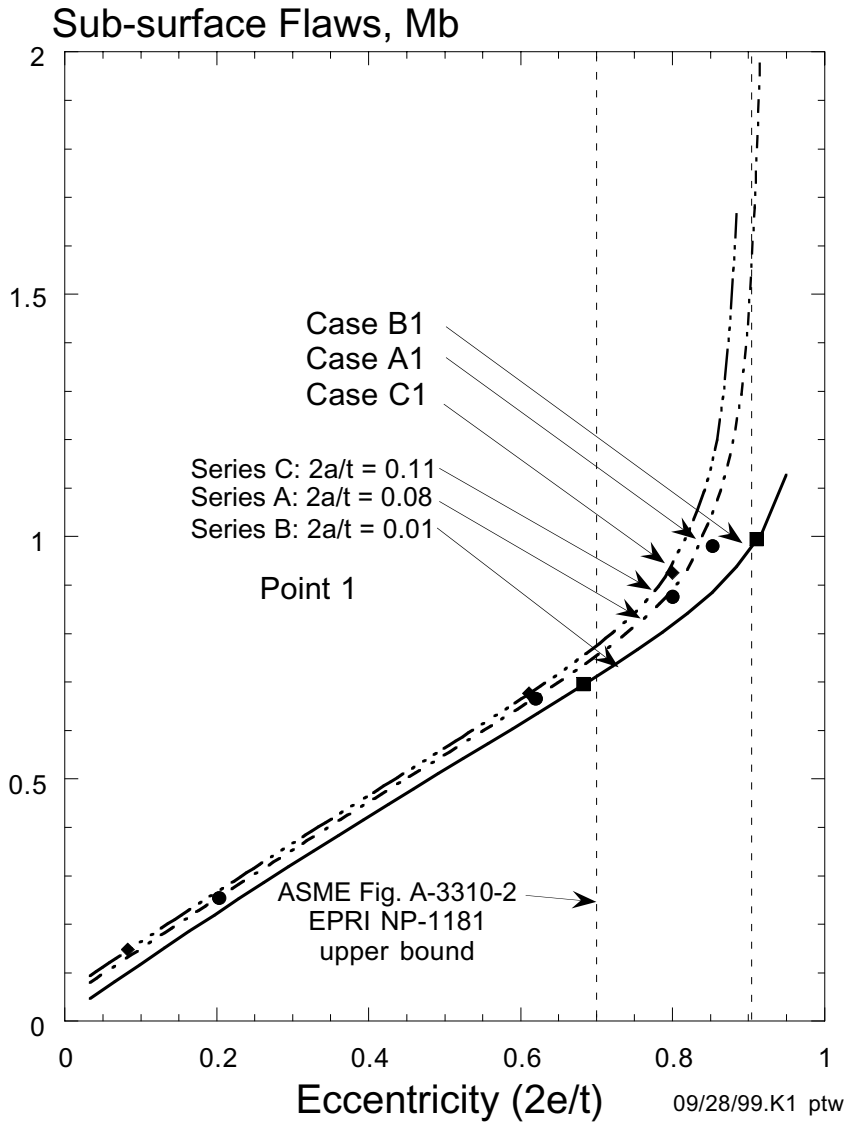

Fig. 14. Bending stress correction factors for analysis matrix.

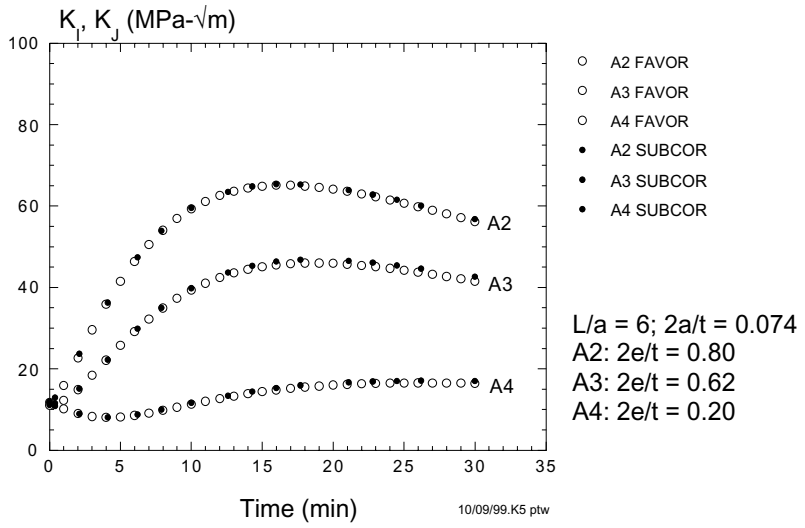

Fig. 15. Benchmarking of FAVOR with SUBCOR based on ASME Section XI subsurface flaw model: Series A embedded flaws.

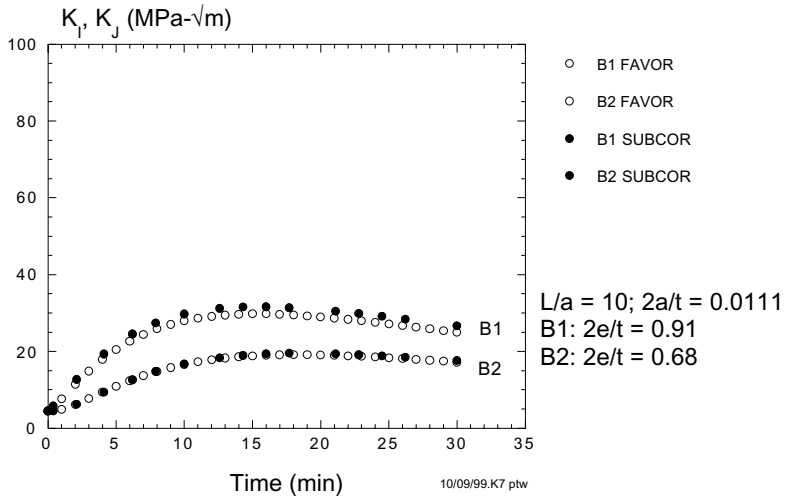

Fig. 16. Benchmarking of FAVOR with SUBCOR based on ASME Section XI subsurface flaw model: Series B embedded flaws.

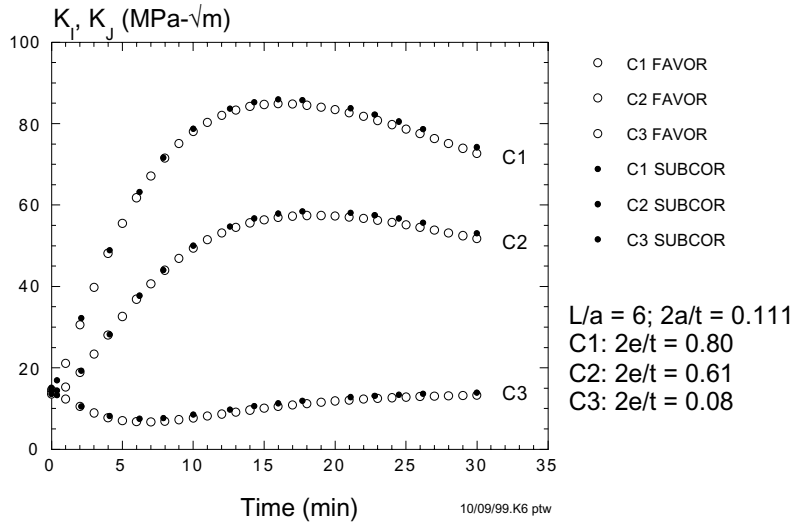

Fig. 17. Benchmarking of FAVOR with SUBCOR based on ASME Section XI subsurface flaw model: Series C embedded flaws.

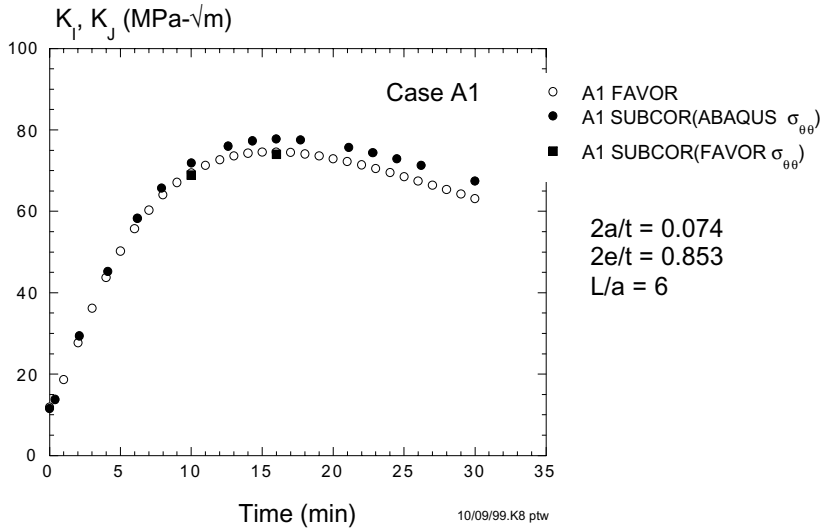

Fig. 18. Benchmarking of FAVOR with SUBCOR based on ASME Section XI subsurface flaw model: Case A1.

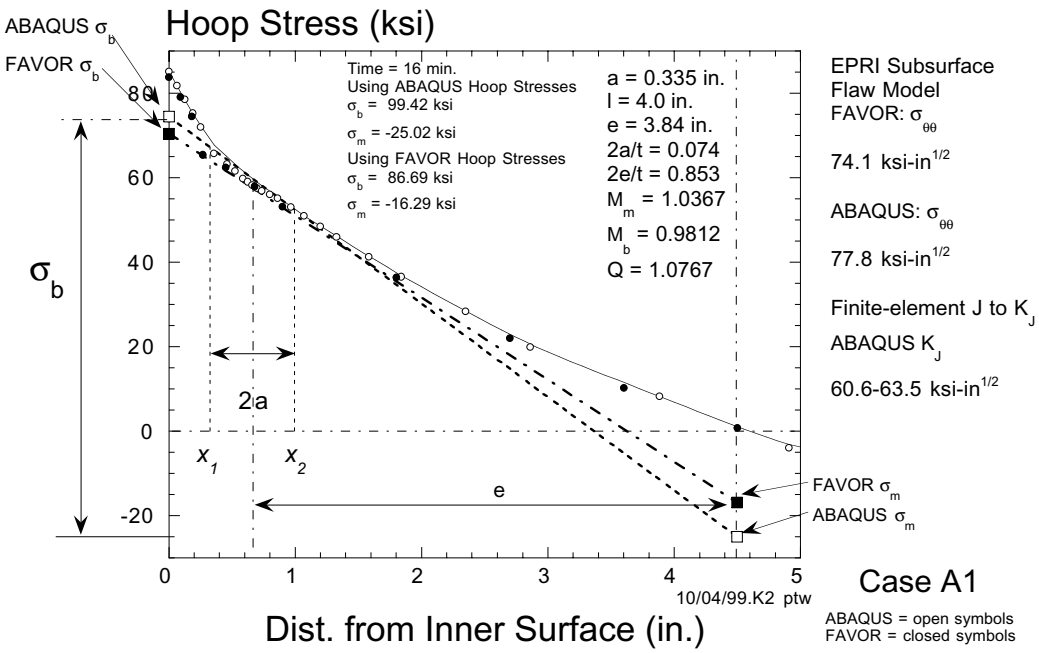

Fig. 19. Comparison of linearization of FAVOR and ABAQUS hoop stress profiles.

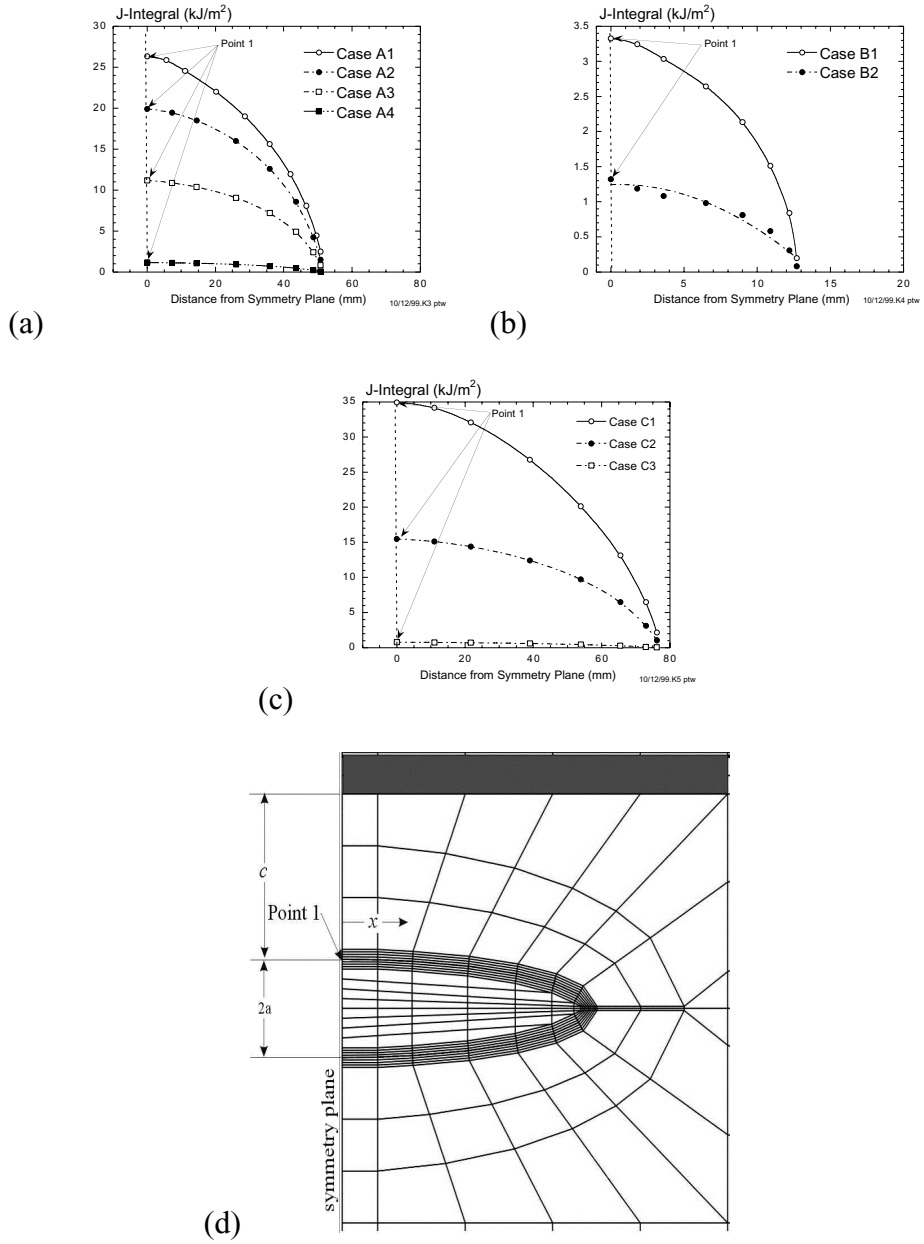

Fig. 20. Profiles of *J*-integrals as a function of distance from vertical symmetry plane for peak times in the PTS transient: (a) Series A, (b) Series B, and (c) Series C; (d) definition of abscissa, *x*, in (a)-(c).

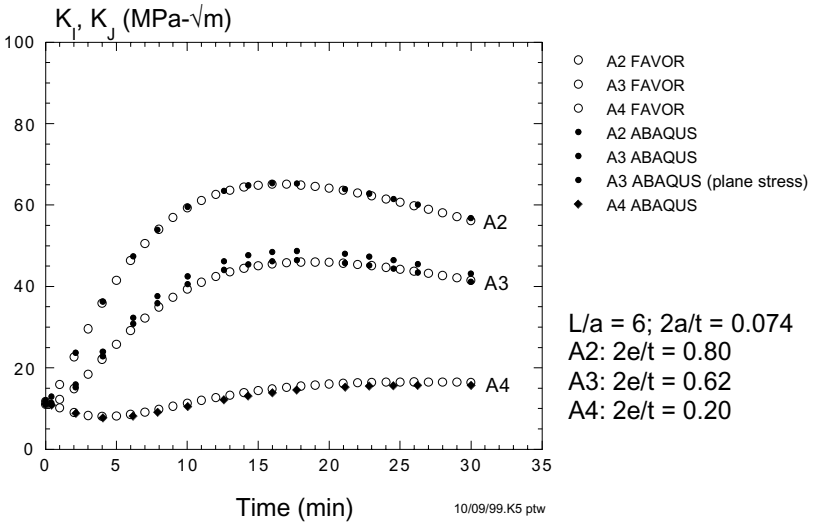

Fig. 21. Benchmarking of FAVOR with 3-dimensional finite-element (ABAQUS) LEFM solutions: Series A embedded flaws.

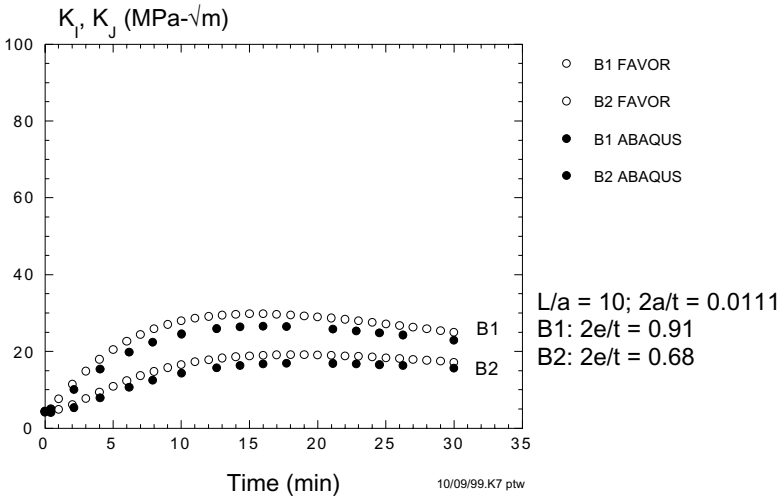

Fig. 22. Benchmarking of FAVOR with 3-dimensional finite-element (ABAQUS) LEFM solutions: Series B embedded flaws.

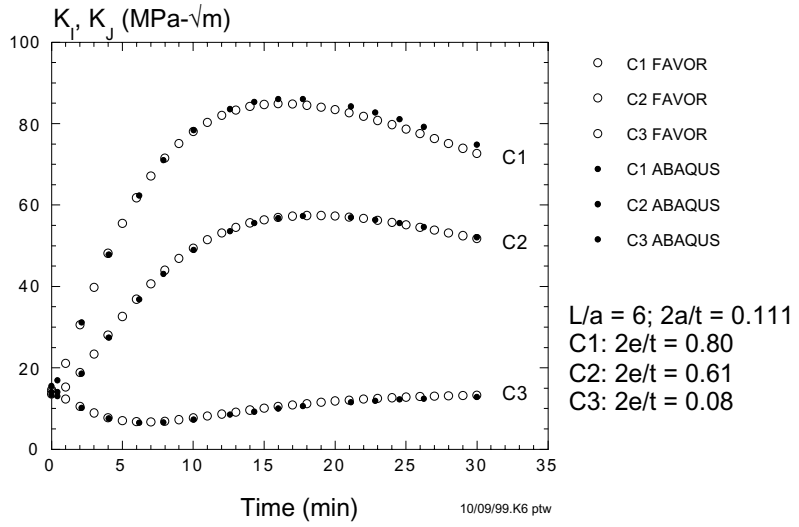

Fig. 23. Benchmarking of FAVOR with 3-dimensional finite-element (ABAQUS) LEFM solutions: Series C embedded flaws.

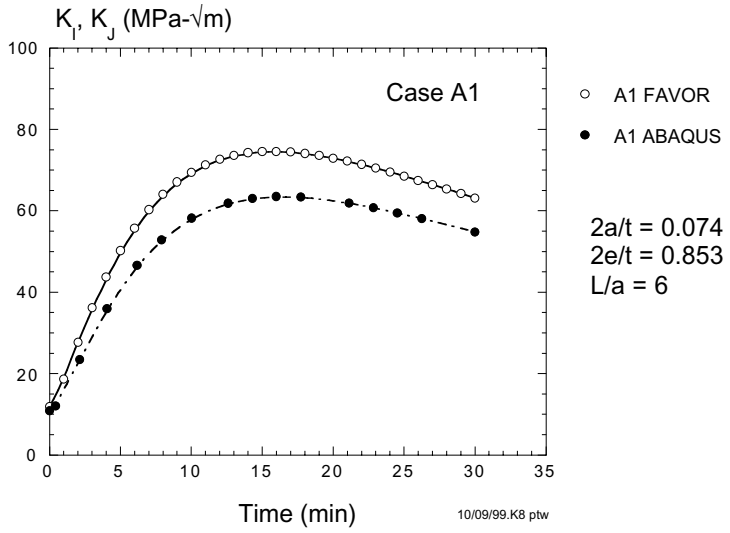

Fig. 24. Benchmarking of FAVOR with 3-dimensional finite-element (ABAQUS) LEFM solutions: Case A1.

APPENDIX

Listing of Subroutines Used in the SUBCOR Code to Calculate Parameters in EPRI Flaw Model

- **subroutine Qflaw**: calculate the Q parameter for semielliptical and elliptical flaws
- **subroutine Mm_subsurface**: calculate the membrane stress correction factor, M_m, for subsurface flaws
- **subroutine Mb_subsurface**: calculate the bending stress correction factor, M_b, for subsurface flaws.

```
!*********************************************************************
!***                                                               ***
!***                             Qflaw                             ***
!***                                                               ***
!***     Evaluate the shape parameter for elliptical flaws         ***
!***     Input:                                                    ***
!***      a = 1/2 flaw minor axis length                           ***
!***      L = flaw major axis length                               ***
!***     Output:                                                   ***
!***      Q = shape parameter                                      ***
!***      Q = -1.0 if L or a/L out of bounds                       ***
!***      Q1 = using IMSL elliptical integral of the second kind   ***
!***      Q2 = using EPRI NP-1181 curve fit                        ***
!***      Q3 = using ASME, Sect. XI, Appendix A curve fit          ***
!***      Bounds                                                   ***
!***      0 < a/L < 0.5, L > 0.0                                   ***
!***     functions called:                                         ***
!***      IMSL function DELE - elliptical integral of second kind  ***
!***    Ref: R. C. Cipolla, Computational Method to Perform the    ***
!***         Flaw Evaluation Procedure as Specified in the ASME    ***
!***         Code, Section XI, Appendix A, EPRI NP-1181, 1979.     ***
!***    Paul T. Williams, Ph.D., P.E.                              ***
!***    Oak Ridge National Laboratory                              ***
!*********************************************************************
      subroutine Qflaw(a,L,Q1,Q2,Q3)
      use setprecision_h
      use numerical_libraries
      implicit none
!-----------------------------------------------------------------------
      real(setpr), intent(IN) :: a,L
      real(setpr), intent(OUT):: Q1,Q2,Q3
!-----------------------------------------------------------------------
      real(setpr)             :: Ek,k,m,pi
      real(setpr),parameter   :: zero = 0.,one=1.,two=2.,four=4.
!-----------------------------------------------------------------------
      pi = four*ATAN(one)
      if ( L > zero ) then
        if ( a < (0.5*L) ) then
!         using IMSL function
          k  = one - four*(a/L)**2
          Ek = DELE( k ) ! Complete elliptic integral of the second kind
          Q1 = Ek*Ek
!         using EPRI NP-1181 curve fit
          m = (one - two*a/L)/(one + two*a/L)
          Q2 = 0.25*pi**2 * ( one + 0.25*m**2 + 0.015625*m**4 +         &
     &         0.00390625*m**6    + 1.5258789e-03*m**8        +         &
     &         7.47680664e-04*m**10 )**2 / (one + m)**2
!         using ASME Sect. XI, Appendix A curve fit
          Q3 = one + 4.593*(a/L)**1.65_setpr
        else
          Q1 = -one
          Q2 = -one
          Q3 = -one
        endif
      else
       Q1 = -one
       Q2 = -one
       Q3 = -one
```

```
      endif
!-----------------------------------------------------------------------
      endsubroutine Qflaw

!*********************************************************************
!***                                                               ***
!***                          Mm_subsurface                        ***
!***                                                               ***
!***  Evaluate the correction factor for subsurface flaw (tension)  ***
!***     Input:                                                    ***
!***      a = 1/2 flaw minor axis length                           ***
!***      e = flaw eccentricity                                    ***
!***      t = wall thickness                                       ***
!***      Pt= Pt1 or Pt2                                           ***
!***     Output:                                                   ***
!***      Mm= correction factor                                    ***
!***      Mm= -1.0 if a/L out of bounds                            ***
!***      Bounds                                                   ***
!***       t > 0.0  a > 0.0                                        ***
!***       2a/t < 1 – 2e/t                                         ***
!***     functions called:                                         ***
!***      NONE                                                     ***
!***    Ref: R. C. Cipolla, Computational Method to Perform the    ***
!***         Flaw Evaluation Procedure as Specified in the ASME    ***
!***         Code, Section XI, Appendix A, EPRI NP-1181, 1979.     ***
!***    Paul T. Williams, Ph.D., P.E.                              ***
!***    Oak Ridge National Laboratory                              ***
!*********************************************************************
      subroutine Mm_subsurface(a,e,t,Mm,Pt)
      use setprecision_h
      use numerical_libraries
      implicit none
!-----------------------------------------------------------------------
      integer,     intent(IN) :: Pt
      real(setpr), intent(IN) :: a,e,t
      real(setpr), intent(OUT):: Mm
!-----------------------------------------------------------------------
      real(setpr),dimension(9):: D
      real(setpr)             :: at,ea
      real(setpr),parameter   :: zero=0.,one=1.,two=2.
!-----------------------------------------------------------------------
      if ( t > zero ) then
         at = two*a/t
      else
         Mm = -one
         return
      endif
      if ( a > zero ) then
         ea = e/a
      else
         Mm = -one
         return
      endif
!
      if ( Pt == 1 ) then
        D(6) = 0.303_setpr
      else
        D(6) = zero
```

```
        ea   = -ea
      endif
!
      D(1) = one
      D(2) = 0.5948_setpr
      D(3) = 0.4812_setpr + 0.7861_setpr*ea + 1.9502_setpr*ea**2
      D(4) = 0.3963_setpr + 0.4207_setpr*ea + 1.8806_setpr*ea**2 +      &
     &       1.6026_setpr*ea**3 + 3.1913_setpr*ea**4
      D(5) = 0.3354_setpr + 0.3199_setpr*ea + 1.8104_setpr*ea**2 +      &
     &       1.4472_setpr*ea**3 + 2.7301_setpr*ea**4 +                  &
     &       3.6902_setpr*ea**5 + 6.8410_setpr*ea**6
!
      if ( (one - two*e/t - at) > zero ) then
        Mm   = D(1) + D(2)*at**2 + D(3)*at**4+D(4)*at**6+D(5)*at**8+    &
     &              D(6)*at**20/SQRT(one - (two*e/t) - at)
      else
        Mm = -one
      endif
!-----------------------------------------------------------------------
      end subroutine Mm_subsurface

!*********************************************************************
!***                                                               ***
!***                          Mb_subsurface                        ***
!***                                                               ***
!***  Evaluate the correction factor for subsurface flaw (bending)  ***
!***                                                               ***
!***     Input:                                                    ***
!***      a = 1/2 flaw minor axis length                           ***
!***      ec= flaw eccentricity                                    ***
!***      t = wall thickness                                       ***
!***      Pt= position flag (1 or 2)                               ***
!***     Output:                                                   ***
!***      Mb= correction factor                                    ***
!***      Mb= -1.0 if a/L out of bounds                            ***
!***      Bounds                                                   ***
!***      0.1 < 2a/t < 0.7                                         ***
!***      0.0 < 2e/t < 0.7                                         ***
!***      2a/t < 1 – 2e/t                                          ***
!***     functions called:                                         ***
!***      NONE                                                     ***
!***    Ref: R. C. Cipolla, Computational Method to Perform the    ***
!***         Flaw Evaluation Procedure as Specified in the ASME    ***
!***         Code, Section XI, Appendix A, EPRI NP-1181, 1979.     ***
!***    Paul T. Williams, Ph.D., P.E.                              ***
!***    Oak Ridge National Laboratory                              ***
!*********************************************************************
      subroutine Mb_subsurface(a,ec,t,Mb,Pt)
      use setprecision_h
      use numerical_libraries
      implicit none
!-----------------------------------------------------------------------
      integer,     intent(IN) :: Pt
      real(setpr), intent(IN) :: a,ec,t
      real(setpr), intent(OUT):: Mb
!-----------------------------------------------------------------------
      real(setpr),dimension(9):: E= (/                                  &
     &  0.84086850,1.5090020, -0.6037780,-0.7731469,0.1294097,          &
```

```
     &  0.88416850,-0.07410377,0.04428577,-0.8338377/)
      real(setpr),dimension(8) :: F =(/                                  &
     & -0.004378676,1.052083, -0.05479575,-0.08603191,0.3805255,         &
     & -0.442080000,-0.1208818,0.03725713/)
      integer                  :: i
      real(setpr)              :: at,et
      real(setpr),parameter    :: zero=0.,one=1.,two=2.
!-----------------------------------------------------------------------
      if ( t > zero ) then
         at = two*a/t
         et = two*ec/t
      else
         Mb = -one
         return
      endif
      if ( at < 0.1_setpr .OR. at > 0.7_setpr ) then
         Mb = -one
         return
      elseif ( et <= 0.0_setpr .OR. er > 0.7_setpr ) then
         Mb = -one
         return
      elseif ( Pt == 1 ) then
         if ( (one - et - at) > zero ) then
           Mb = E(1) + ( E(2)*et + E(3)*et**2 + E(4)*et*at  +            &
     &          E(5)*at*et**2    + E(6)*at    + E(7)*at**2  +            &
     &          E(8)*et*at**2    + E(9) ) /                              &
     &          SQRT(one - et - at)
         else
           Mb = -one
           return
         endif
      else
         Mb = F(1) + F(2)*et + F(3)*et**2    + F(4)*at*et +              &
     &        F(5)*at*et**2  + F(6)*at       + F(7)*at**2 +              &
     &        F(8)*et*at**2
      endif
!-----------------------------------------------------------------------
      end subroutine Mb_subsurface
```

Internal Distribution

1-5. B. R. Bass
6. W. G. Craddick
7. T. L. Dickson
8. D. M. Hetrick
9. M. A. Kuliasha
10. S. K. Iskander
11. W. J. McAfee
12. R. K. Nanstad
13-14. C. E. Pugh
15. T. M. Rosseel
16. J. J. Simpson
17. M. A. Sokolov
18-22. P. T. Williams
23. Laboratory Records

External Distribution

24. W. H. Bateman, NRR, U.S. Nuclear Regulatory Commission, MS O7 D4, Washington, D.C. 20555-0001
25. R. H. Dodds, 3140 Newmark Laboratory, 205 North Matthews, Urbana, IL 61801
26. C. J. Fairbanks, RES/DET/MEB, U.S. Nuclear Regulatory Commission, MS T-10 E10, Washington, D.C. 20555-0001
27. E. M. Hackett, RES/DET/MEB, U.S. Nuclear Regulatory Commission, MS T-10 E10, Washington, D.C. 20555-0001
28. J. A. Joyce, U.S. Naval Academy, Mechanical Engineering Department, MS 11C, 590 Hollway Road, Annapolis, MD 21402
29-33. M. T. Kirk, RES/DET/MEB, U.S. Nuclear Regulatory Commission, MS T-10 E10, Washington, D.C. 20555-0001
34-35. S. N. Malik, RES/DET/MEB, U.S. Nuclear Regulatory Commission, MS T-10 E10, Washington, D.C. 20555-0001
36. M. E. Mayfield, RES/DET, U.S. Nuclear Regulatory Commission, MS T-10 E10, Washington, D.C. 20555-0001
37. M. A. Mitchell, NRR, U.S. Nuclear Regulatory Commission, MS O7 D4, Washington, D.C. 20555-0001
38. C. G. Santos, RES/DET/MEB, U.S. Nuclear Regulatory Commission, MS T-10 E10, Washington, D.C. 20555-0001
39. W. J. Shack, Energy Technology Division, Argonne National Laboratory, 9700 S. Cass Avenue, Argonne, IL 60439
40. R. L. Tregoning, Fatigue and Fracture Branch, Carderock Division, Naval Surface Warfare Center, 9500 McArthur Blvd., West Bethesda, MD 20817-5700
41. K. R. Wichman, NRR, U.S. Nuclear Regulatory Commission, MS O7 D4, Washington, D.C. 20555-0001